

PAPER • OPEN ACCESS

Metal assisted photochemical etching of 4H silicon carbide

To cite this article: Markus Leitgeb *et al* 2017 *J. Phys. D: Appl. Phys.* **50** 435301

View the [article online](#) for updates and enhancements.

Related content

- [Enhanced optical performance of electrochemically etched porous silicon carbide](#)
N Naderi, M R Hashim, K M A Saron *et al.*
- [Anodic etching of SiC in alkaline solutions](#)
D H van Dorp, J L Weyher and J J Kelly
- [Galvanically coupled gold/SOI microstructures in hydrofluoric acid electrolytes](#)
C R Becker, D C Miller and C R Stoldt

Recent citations

- [Editors' Choice—A Cellular Automaton Based Interpretation of Metal Assisted Photochemical Porosification of 4H Silicon Carbide](#)
Markus Leitgeb *et al*



IOP | ebooks™

Bringing you innovative digital publishing with leading voices to create your essential collection of books in STEM research.

Start exploring the collection - download the first chapter of every title for free.

Metal assisted photochemical etching of 4H silicon carbide

Markus Leitgeb¹, Christopher Zellner¹, Michael Schneider¹,
Stefan Schwab², Herbert Hutter² and Ulrich Schmid¹

¹ Institute of Sensor and Actuator Systems, TU Wien, Gusshausstraße 27-29, Vienna 1040, Austria

² Institute of Chemical Technology and Analytics, TU Wien, Getreidemarkt 9/164, Vienna 1040, Austria

E-mail: markus.leitgeb@tuwien.ac.at

Received 6 June 2017, revised 21 August 2017

Accepted for publication 30 August 2017

Published 27 September 2017




Abstract

Metal assisted photochemical etching (MAPCE) of 4H–silicon carbide (SiC) in Na₂S₂O₈/HF and H₂O₂/HF aqueous solutions is investigated with platinum as metallic cathode. The formation process of the resulting porous layer is studied with respect to etching time, concentration and type of oxidizing agent. From the experiments it is concluded that the porous layer formation is due to electron hole pairs generated in the semiconductor, which stem from UV light irradiation. The generated holes are consumed during the oxidation of 4H–SiC and the formed oxide is dissolved by HF. To maintain charge balance, the oxidizing agent has to take up electrons at the Pt/etching solution interface.

Total dissolution of the porous layers is achieved when the oxidizing agent concentration decreases during MAPCE. In combination with standard photolithography, the definition of porous regions is possible. Furthermore chemical micromachining of 4 H–SiC at room temperature is possible.

Keywords: metal assisted etching, silicon carbide, micromachining, porous silicon carbide

 Supplementary material for this article is available [online](#)

(Some figures may appear in colour only in the online journal)

1. Introduction


Nowadays there exists a variety of methods to produce porous silicon from single crystalline wafers. The most common methods are electrochemical etching [1], stain etching [2] and metal assisted etching [3, 4]. A large variety of possible application scenarios for such porous layers is reported in literature. Porous silicon can be used as sacrificial layer in the fabrication of MEMS devices. There it is either chemically removed [5, 6] or the porous structure reorganizes under inert gas atmosphere at high temperatures [7]. Another application is in the field of biosensors where porous layers with a homogeneous porosity depth profile are needed [8]. Contrary to this

application a smoothly increasing refractive index of the porous layer is recommended for the fabrication of efficient antireflective layers [9]. Porous silicon offers a high surface to volume ratio, thus being most beneficially used in super capacitors [10], chemical sensors [11] or explosive devices [12, 13].

There are, however, certain limitations for porous silicon. In harsh environments, at high temperatures and in alkaline electrolyte solutions, porous silicon cannot be used. It degrades chemically (i.e. due to oxidation) or even dissolves. To exploit its full benefit under such conditions, the surface has to be covered with a stable and dense protective layer [14].

Porous silicon carbide is regarded as promising alternative due to its higher temperature stability and enhanced chemical inertness.

For successful implementation of porous silicon carbide within MEMS devices, the fundamentals of pore formation

 Original content from this work may be used under the terms of the [Creative Commons Attribution 3.0 licence](#). Any further distribution of this work must maintain attribution to the author(s) and the title of the work, journal citation and DOI.

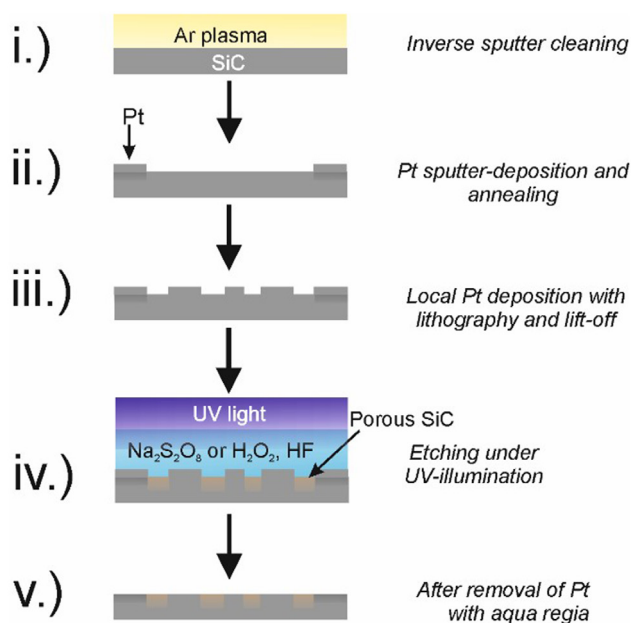


Figure 1. Process flow chart for metal assisted photochemical etching (MAPCE) of silicon carbide.

need to be understood. Moreover the capability to monitor the etching reaction by electrical probing is desirable.

In this study metal assisted photochemical etching (MAPCE) is utilized for defined porosification of 4H-SiC. In this approach, a thin film of noble metal is deposited on the SiC surface. Next, the sample is placed into an etching solution, containing hydrofluoric acid and an oxidation agent such as Na₂S₂O₈ or H₂O₂. The noble metal acts as cathode while the surface exposed to the etchant is the corresponding anode. The oxidant is reduced at the cathode and SiC is oxidized at the anode. The generated oxide is dissolved with HF [15].

Recent experiments showed that a decreased contact resistance at the Pt/4H-SiC junction enhances the electron flow during etching. This result allowed successful porosification of 4H-SiC substrates having different bulk resistivities [16].

Despite the results reported in literature, the knowledge about MAPCE with respect to 4H-SiC is still very poor. Even in the laboratory scale it has not yet been established as a reliable method to produce porous SiC.

The objective of this paper is to introduce MAPCE as a reliable and simple technique for the generation of uniform and highly porous 4H-SiC layers. In addition, this study also aims to contribute to the fundamental understanding of MAPCE when applied to this wide bandgap semiconductor.

2. Experimental details

For all experiments $1 \times 1 \text{ cm}^2$ n-type, nitrogen doped 4H-SiC samples with a resistivity of $(0.012\text{--}0.025) \Omega \cdot \text{cm}$ were used. The process flow chart for the performed experiments is illustrated in figure 1. Initially the samples were cleaned consecutively in acetone, isopropanol and ethanol for 5 min. Afterwards an inverse sputter cleaning procedure was carried out (step i). This cleaning step lasted for 240s at a plasma power of 200 W, applying a ‘Von Ardenne’ sputter equipment

(LS730S). All sputter deposition experiments described in this study were performed with this equipment. Next 300 nm of Pt were sputtered on the samples (step ii). Prior investigations showed the importance of the Pt/4H-SiC junction properties [16]. To enable reliable etching, the contact resistance at this interface has to be decreased. Therefore the samples were annealed in a Nabertherm L9/11/SKM oven under Argon flow of 40 l h^{-1} starting at $800 \text{ }^\circ\text{C}$ with a subsequent 30 min ramp up to $1100 \text{ }^\circ\text{C}$. This peak temperature was held for 5 min.

The annealing process lead to surface roughening of 4H-SiC at Pt-covered areas. Therefore (step ii) was not performed across the whole sample surface, only a strip near the sample edge region was used, covering about 10% of the sample’s surface.

Next, a second layer of 100 nm Pt was sputter deposited and patterned using lift-off, providing Pt on the areas with a smooth surface characteristic (step iii).

The samples were immersed in an etching solution containing an oxidizing agent (Na₂S₂O₈ or H₂O₂) and HF (step iv). The HF concentration in all performed experiments was 1.31 mol l^{-1} , while the concentrations of the oxidants varied. The necessary UV irradiation was provided by a custom built UV source utilizing an 18 W UV-C low pressure mercury vapor lamp (peak intensity at 254 nm). The volume of the etching solution was 1.2 ml and the distance between the sample and the light source was 0.7 cm. During all experiments the C-face of the samples was porosified.

After etching all samples were examined with a Hitachi SU8030 scanning electron microscope using acceleration voltages ranging between 2 and 5 kV. The redox potentials were recorded using a Pt wire that touched the sputter deposited Pt on the samples. This served as sensing electrode. As reference a mercury/mercurous-sulfate electrode filled with saturated K₂SO₄ was used. The redox potentials were measured under room light conditions.

FT-IR measurements were performed in attenuated total reflection (ATR) mode. Therefore a Bruker Tensor FT-IR spectrometer was used.

TOF SIMS depth profiles were acquired using a TOF-SIMS 5 (IonToF GmbH, Münster, Germany). A 25 keV Bi⁺ primary ion beam was used for analysis (high current bunched mode [17]). For sputtering a 2 keV Cs⁺ beam was used. The analysis area was set to $50 \times 50 \mu\text{m}$ with a pixel resolution of 128×128 and the crater size to $400 \times 400 \mu\text{m}$. The measurements were carried out in negative ion mode using the interlaced mode with a cycle time of $100 \mu\text{s}$. Low energy electron flooding (21 V) was applied.

3. Results and discussion

3.1. Preface

Current theory states that with increasing porosity the porous structure is mostly covered by the semiconductor-electrolyte space charge layer [18, 19]. With ongoing etching time most of the oxidant should be reduced. Thus the redox potential as an indicator for the Fermi level of the etching solution should decrease [20]. To achieve a fast decay of the oxidant, small

volumes (1.2 ml) of etching solution were used. Pore formation should stop when all of the oxidizing agent is reduced. Furthermore it was assumed, that the resulting porous layer should have a homogenous porosity depth profile because the space charge layer limits the final degree of porosity. This would allow to control the degree of porosity across the porous layer, while the progress of the etching reaction could be recorded with redox potential measurements. The problem of heat generation would be minimized with a low pressure mercury lamp that emits no infrared radiation. Moreover low etchant volumes are of economic interest, especially when highly toxic etching solutions are used. The experiments were carried out with either H_2O_2 or $\text{Na}_2\text{S}_2\text{O}_8$ to investigate the influence of the oxidizing agent type on MAPCE. To the best of the author's knowledge, H_2O_2 has not yet been successfully used as oxidizing agent during MAPCE of SiC.

3.2. Evolution of the porous layer

In this section the evolution of the porous layer during etching is presented with varying oxidizing agent types (H_2O_2 or $\text{Na}_2\text{S}_2\text{O}_8$) and concentrations. Porous layers were formed at 25 μm and 50 μm square areas defined by photolithography.

The porosified area of each sample was 0.11 cm^2 . The etching times ranged between 15 and 150 min and the C-face was exposed to the etching solution.

First the experimental results with H_2O_2 containing solutions are presented, then those with $\text{Na}_2\text{S}_2\text{O}_8$. Finally, all results are evaluated and discussed.

3.2.1. Experiments with H_2O_2 . Figure 2 shows the evolution of the etching depth and the redox potential with respect to etching time. After 60 min the total etching depth, as well as the redox potential becomes relatively constant. This is attributed to the decay of H_2O_2 due to photolysis (equation (1)) [21] in the etching solution with time.



When all the H_2O_2 is decomposed, no further etching into depth is observed. This behavior is illustrated in figure 3. At first the total etching depth increases until it becomes relatively constant. This behavior is accompanied by the formation of a defined etching front. When the total etching depth does not increase anymore, total dissolution of porous 4H-SiC takes place. This is an unexpected behavior and is discussed below in this section after the presentation of additional results (see section 3.3).

Next the influence of a higher H_2O_2 concentration (i.e. 0.15 mol l^{-1} instead of 0.04 mol l^{-1}) is presented. Qualitatively the same result was obtained as can be seen in figures 4 and 5. The redox potential as well as the total etching depth become constant with ongoing etching time.

Beside these similarities there are also differences when the H_2O_2 concentration is increased. At longer etching times a so-called line of breakage forms (see figure 5(d)). This means that total dissolution takes place at the bottom of the porous layer, instead at the top surface. So the upper porous layer is

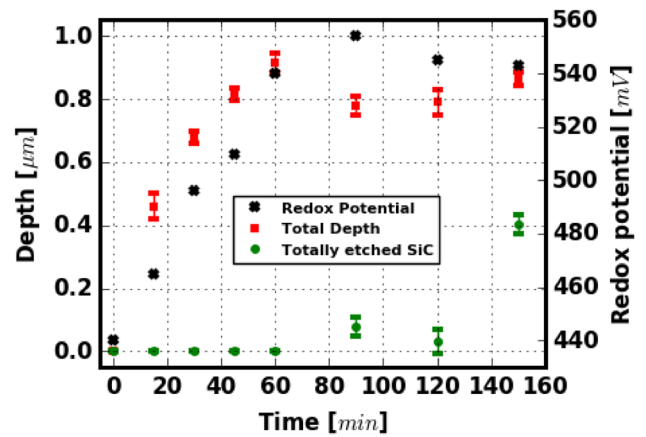


Figure 2. Etching depth and redox potential versus time. Etching solution: 1.2 ml of 0.04 mol l^{-1} H_2O_2 in 1.31 mol l^{-1} HF, while the C-face is exposed to the etchant. The error bars represent the standard deviation from 10 measurements.

protected from further etching because total dissolution starts at its bottom.

3.2.2. Experiments with $\text{Na}_2\text{S}_2\text{O}_8$. Now the results with $\text{Na}_2\text{S}_2\text{O}_8$ as oxidizing agent are presented. The etching depth and redox potential characteristics are illustrated in figure 6 (0.04 mol l^{-1} $\text{Na}_2\text{S}_2\text{O}_8$) and figure 8 (0.15 mol l^{-1} $\text{Na}_2\text{S}_2\text{O}_8$). The corresponding SEM micrographs are shown in figures 7 and 9.

The same statements as for the samples etched with H_2O_2 based etchants (see section 3.2.1) can be made. After a certain time all the oxidizing agent is consumed due to photolysis (equation (2)) [22] and the total etching depth does not increase anymore (see figure 6). During the experiment with 0.15 mol l^{-1} $\text{Na}_2\text{S}_2\text{O}_8$ also a decrease of the redox potential could be monitored. This indicates the decay of $\text{Na}_2\text{S}_2\text{O}_8$ in the etching solution. This is contrary to the samples etched with H_2O_2 , where the redox potential increased. This phenomenon has been studied and the results are shown in the supplementary material S1 (stacks.iop.org/JPhysD/50/435301/mmedia).



After pore formation into depth had stopped, also total dissolution of the porous layer took place. However in no experiment with $\text{Na}_2\text{S}_2\text{O}_8$, the formation of a line of breakage could be observed. An increase of the $\text{Na}_2\text{S}_2\text{O}_8$ concentration from 0.04 mol l^{-1} to 0.15 mol l^{-1} yielded an etching process still ongoing into depth after 150 min, so that total dissolution was not observed (see figures 8 and 9). This is attributed to the presence of a not reduced oxidizing agent in the etching solution. However, etching at the top surface of the porous layer stopped, as is shown by an analysis of the pore size distribution in this region. Figure 10 shows the modal pore area (i.e. the pore area that appears most often in the pore distribution) after different etching times for the experiments with 0.15 mol l^{-1} $\text{Na}_2\text{S}_2\text{O}_8$ (see figures 8 and 9). At first the average pore size increases almost linearly with time. The sharp increase represents individual pores that connect to larger clusters. From this characteristic point on, the pore size stays relatively

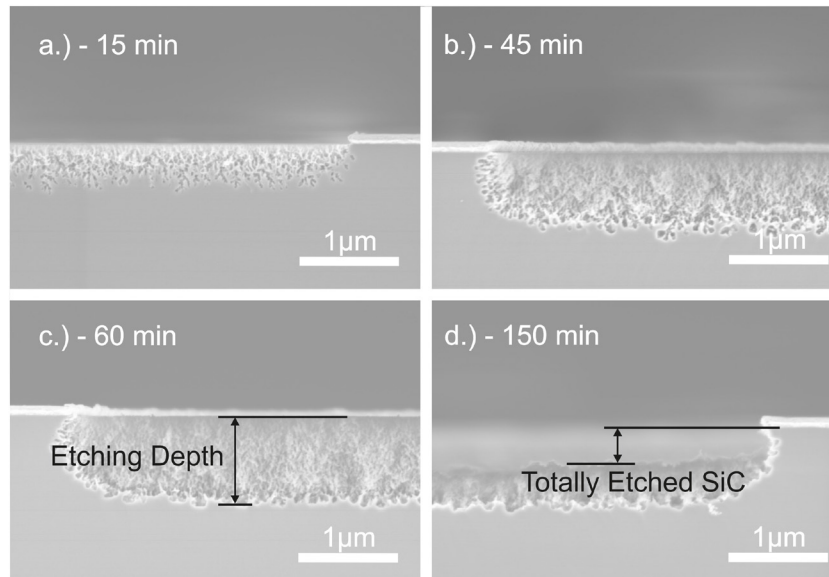
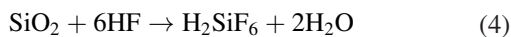


Figure 3. Evolution of the porous layer with increasing etching time. Etching solution: 1.2 ml of 0.04 mol l⁻¹ H₂O₂ in 1.31 mol l⁻¹ HF, while the C-face is exposed to the etchant.

constant, indicating a drastic drop of the etching rate. This demonstrates that etching of the porous layer stops at the highly porous regions at the top while pore formation into depth still proceeds. More details about the pore size evaluation can be found in the supplementary material S2.

3.3. Discussion

So far the experimental data allow several statements about MAPCE of 4H-SiC. No increased etching depth was observed near the deposited Pt. Furthermore, when UV light is focused onto the sample with a light-wave cable, the etching depth is lower in the vicinity of the sputter deposited Pt, than in regions being further away. So it can be concluded that the electron hole pair generation is done by the UV light irradiation. The UV light generated h⁺ initiate the oxidation of SiC (see equation (3)). The formed oxide is then dissolved by HF (see equation (4)). [15, 16]



This is in contrast to metal assisted etching of other semiconductors like silicon [3] or InP [23] where the oxidant creates h⁺ in the semiconductor and etching is enhanced near the metallic cathode.

Despite this difference, the role of the deposited Pt is to serve as anode; without Pt no etching could be observed. The oxidizing agent serves as electron consumer during etching and takes up electrons at the Pt/etching solution interface. In agreement with this assumption, an etching experiment with deposited Pt and just HF in the etching solution showed only surface roughening. Altogether the following statements can be made: the UV light irradiation generates electron hole pairs. When the holes are responsible for the oxidation of SiC, charge balance must be maintained for etching to proceed.

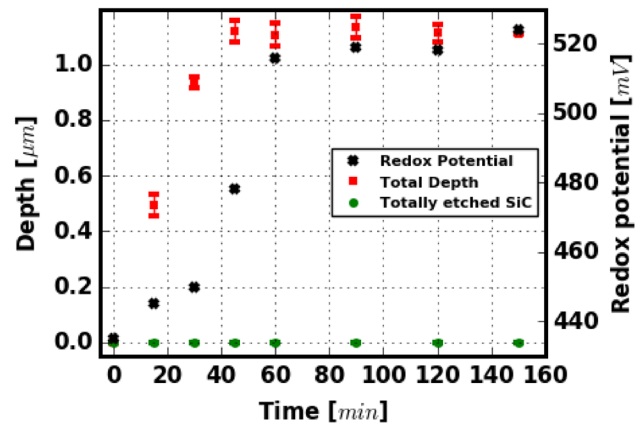


Figure 4. Etching depth and redox potential versus time. Etching solution: 1.2 ml of 0.15 mol l⁻¹ H₂O₂ in 1.31 mol l⁻¹ HF, while the C-face is exposed to the etchant. The error bars represent the standard deviation from 10 measurements.

This is done by the oxidizing agent at the Pt cathode, which is reduced and takes up electrons as is shown in equation (5)



Basically, the etching depth is lower for experiments performed with higher Na₂S₂O₈ (compare figure 6 with figure 8) concentration. This is explained with a decreased UV light intensity that hits the sample, due to a higher oxidizing agent concentration. So the oxidizing agent concentration and the UV light intensity are the main factors competitively controlling the etching rate during MAPCE.

Prior to the experiments presented in this study, it was assumed, that with proceeding etching time the porosity in the layers should become more homogeneous and uniform; the space charge layer formed at the electrolyte semiconductor junction should limit the final degree of porosity [18]. This was confirmed with our experiments, as can be seen in figures 3, 5 and 7.

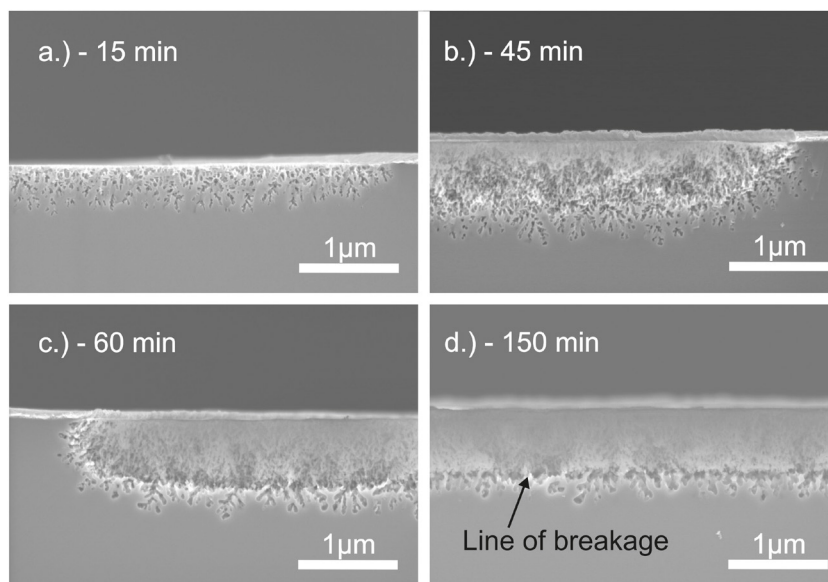


Figure 5. Evolution of the porous layer with increasing etching time. Etching solution: 1.2 ml of 0.15 mol l⁻¹ H₂O₂ in 1.31 mol l⁻¹ HF, while the C-face is exposed to the etchant.

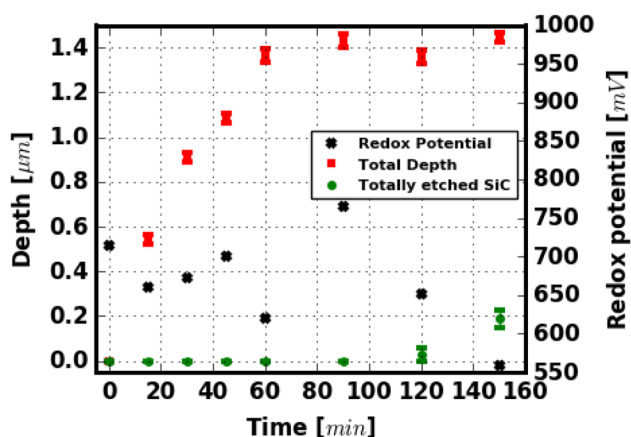


Figure 6. Etching depth and redox potential versus time. Etching solution: 1.2 ml of 0.04 mol l⁻¹ Na₂S₂O₈ in 1.31 mol l⁻¹ HF, while the C-face is exposed to the etchant. The error bars represent the standard deviation from 10 measurements.

Furthermore, an evaluation of the surface pore size showed that there is a passivating effect that protects the upper part of the porous layer from further etching. This passivating effect can also be attributed to the space charge layer at the electrolyte semiconductor junction. With increasing porosity the insulating effect of the space charge layer becomes more dominant and the etching rate slows down.

The experiments have also revealed that this passivating effect is only present under certain experimental conditions. At the later stages of etching when the oxidizing agent concentration is low, total dissolution occurs and the passivating effect is lost.

This indicates that the oxidizing agent concentration is the main factor that is responsible for total dissolution of porous SiC. When the oxidizing agent concentration decreases, the Fermi level of the etching solution increases [24]. As a consequence, the width of the space charge layer decreases in n-type SiC and thus the insulating effect is

reduced. Another explanation is that with increased oxidation rate the amount of surface states is raised as well. Konstantinov *et al* [18] claimed that the surface states pin the Fermi level during anodic etching of SiC and control the width of the space charge layer. This theory is supported by the formation of a line of breakage when using H₂O₂. The total dissolution starts at the bottom of the porous layer (see figure 5). Such an underetching of the porous layer can only be explained by a chemical passivation of the surface of the porous material.

In summary, it can be concluded that MAPCE is controlled by two competing factors: the oxidizing agent concentration and the UV light intensity. The effect of total dissolution can be explained with a decreased width of the space charge layer in the porous SiC with increasing etching time.

4. Chemical composition of the porous layers

Since little knowledge about MAPCE of 4H-SiC is available, the chemical composition of the prepared porous layers was investigated. Furthermore in the previous section it was stated that surface states are responsible for the effect of total dissolution. A chemical analysis of the porous layers can give information about their surface termination. The etched area during the experiments presented in this section was 0.9 cm². First ATR-FTIR measurements were performed to investigate which functional groups are generated during MAPCE. Then TOF-SIMS depth profiling was carried out to assign the observed peaks in the IR spectra. MAPCE was done in time intervals of 30 min. After each interval the old etching solution was replaced by a fresh one to prevent total dissolution. By doing so, the thickness of the porous layers could be increased and clearly identifiable peaks in the IR spectra were obtained. Experiments were performed with H₂O₂ or Na₂S₂O₈ as oxidizing agent while the concentration was in both cases 0.15 mol l⁻¹.

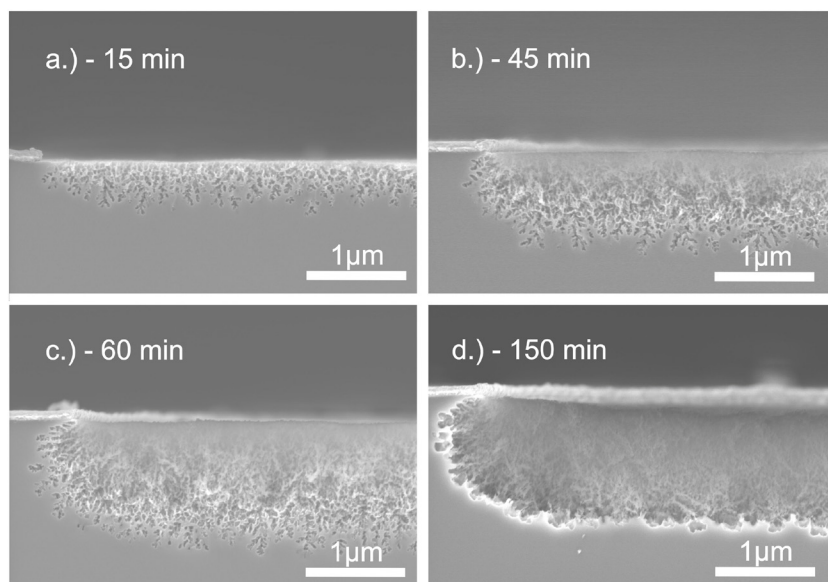


Figure 7. Evolution of the porous layer with etching time. Etching solution: 1.2 ml of $0.04 \text{ mol l}^{-1} \text{ Na}_2\text{S}_2\text{O}_8$ in $1.31 \text{ mol l}^{-1} \text{ HF}$, while the C-face is exposed to the etchant.

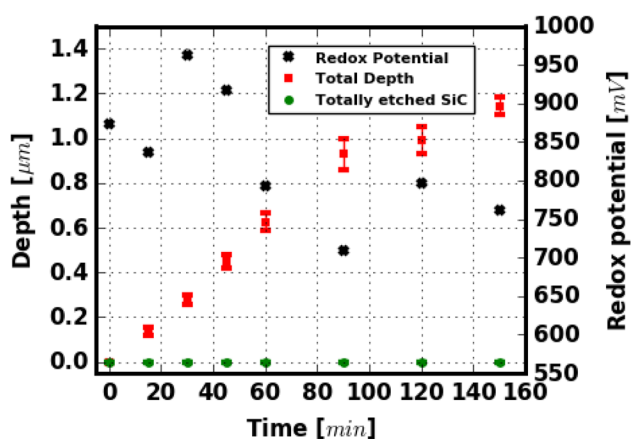


Figure 8. Etching depth and redox potential versus time. Etching solution: 1.2 ml of $0.15 \text{ mol l}^{-1} \text{ Na}_2\text{S}_2\text{O}_8$ in $1.31 \text{ mol l}^{-1} \text{ HF}$, while the C-face is exposed to the etchant. The error bars represent the standard deviation from 10 measurements.

4.1. Experiments with H_2O_2

In figure 11(a), the IR spectra (after baseline subtraction) of samples are presented where MAPCE was performed with H_2O_2 as oxidizing agent, while figures 11(b) and (c) allow enlarged views on the same spectra. The not etched 4H-SiC sample shows characteristic peaks at 810 cm^{-1} and 950 cm^{-1} which are assigned to the TO SiC phonons and LO SiC phonons [25]. The small peaks at 1972 cm^{-1} , 2030 cm^{-1} and 2157 cm^{-1} are assigned to multi phonon absorptions [26, 27]. These features vanish with increasing etching time and new peaks appear, due to the MAPCE process. There is a peak at around 1020 cm^{-1} and a triple peak in the region of 2900 cm^{-1} . To assign the peaks to functional groups, a TOF-SIMS depth profile was recorded from a sample that had been etched for 180 min (see figure 12). F^- as well as O^- related signals were detected. Both characteristics tend to decrease with depth before a relative maximum occurs.

Finally the signal intensity almost vanishes for both F^- and O^- . The $^{30}\text{Si}^-$ isotope signal is given for comparison reasons. There is no clear maximum in the $^{30}\text{Si}^-$ characteristic. The observed features can be interpreted as follows: the F^- as well as the O^- signal decreases with sputter time because the surface-near regions were exposed to the etching solution for a longer time. The local maxima at approximately 50 min of sputter time are related to the active zone during etching. This is shown in figure 13. At the surface-near regions of the porous layer, the etching rate is low due to the passivating effect of the space charge layer. Below is an active zone where etching into depth takes place. Hence an increased amount of O^- and F^- is detected. Simultaneously the intensity of the $^{30}\text{Si}^-$ signal decreases because of a gradually decreasing porosity within the active zone. This is in agreement with findings presented in the previous section; at the top of the porous layer etching stops while pore formation into depth still takes place (see figures 8 and 10). The Si^- as well as the C^- related ion signals were in the upper detector compliance limit (not shown in figure 12). Hence it can be reasoned that most of the porous layer is still SiC. With this elemental information, peak assignment of the spectra in figure 11 is done. The first peak at around 1020 cm^{-1} is assigned to Si–O–Si stretching vibrations [28]. This peak has a shoulder at 985 cm^{-1} which is assigned to SiF_2 stretching vibrations [29, 30]. The triple peak centered at around 2900 cm^{-1} is due to $\text{sp}^3 \text{ C-H}_2$ stretching (i.e. 2852 cm^{-1} symmetric and 2921 cm^{-1} asymmetric) and $\text{sp}^3 \text{ C-H}_3$ asymmetric stretching (2956 cm^{-1}) [28].

The findings support the stated mechanism of MAPCE described by equations (3) and (4), since Si–O–Si vibrations are identified in the IR spectra. According to the proposed mechanism, silicon carbide is first oxidized and then dissolved by HF. So far, this has been just a hypothesis, but not proven by experiments [15, 16]. The results also show that there is fluoride present in the porous layer after etching. Based on this knowledge it is not possible to formalize a

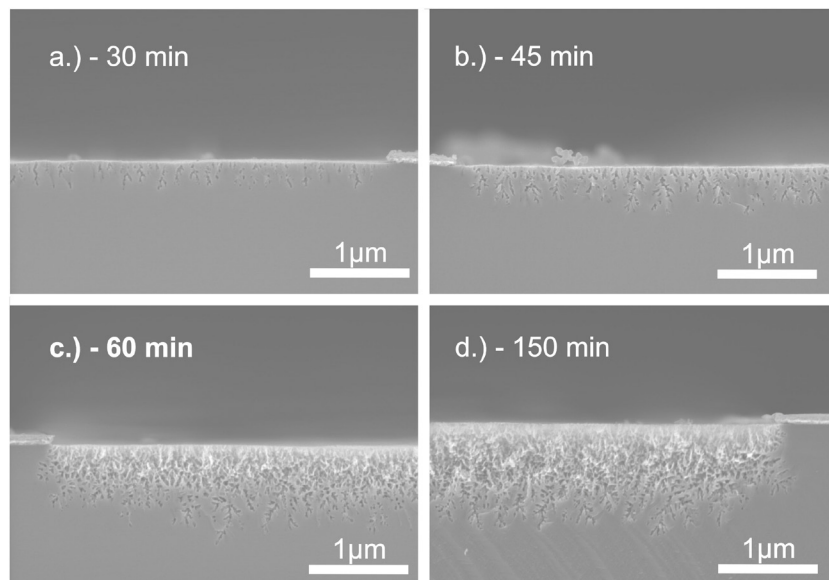


Figure 9. Evolution of the porous layer with etching time. Etching solution: 1.2 ml of 0.15 mol l⁻¹ Na₂S₂O₈ in 1.31 mol l⁻¹ HF, while the C-face is exposed to the etchant.

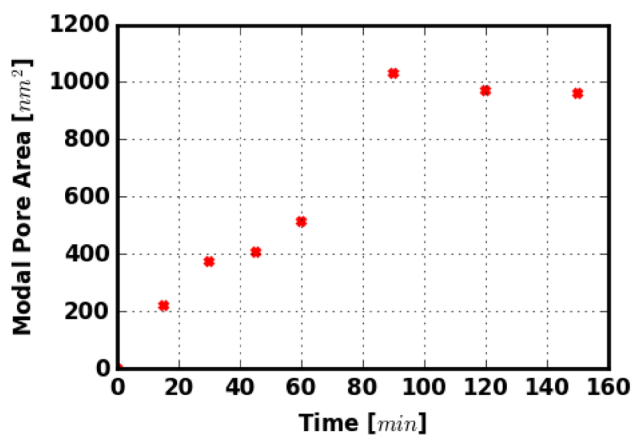


Figure 10. Modal pore area after different etching times. Etching solution: 1.2 ml of 0.15 mol l⁻¹ Na₂S₂O₈ in 1.31 mol l⁻¹ HF, while the C-face is exposed to the etchant.

detailed mechanism of MAPCE, but it is possible that in addition to H₂O, F⁻ serves as nucleophilic species during oxidation and direct dissolution of SiC like in the case of Si takes place [31]. Such a behavior has been suggested by Lauermaun *et al* for anodic etching of SiC [32]. Finally, the C-H_x vibrations are interpreted as follows: Once the oxidation products are dissolved, the pure SiC surface remains, terminated with hydrogen atoms.

Furthermore, no indications for the presence of a carbon rich layer could be found, which is often mentioned in reports related to electrochemical etching of SiC [25, 33]. Peaks between 1200cm⁻¹ and 1800cm⁻¹ in the IR spectrum are attributed to C-C vibrations [34], while other authors label them as N-H vibrations (nitrogen from the doping of SiC) [35]. Such peaks could not be observed during the presented experiments. This shows that the surface termination is different from the one obtained from pure electrochemical

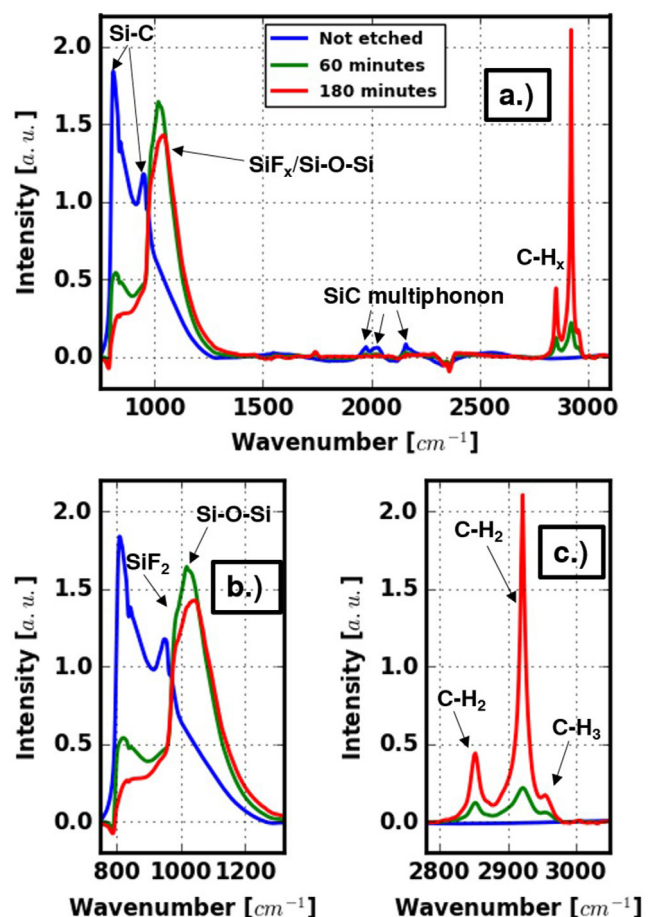


Figure 11. ATR-FTIR spectra of samples etched in 30 min MAPCE periods. Etching solution: 1.2 ml of 0.15 mol l⁻¹ H₂O₂ in 1.31 mol l⁻¹ HF. During etching, the C-face was exposed to the etchant, while the etched area was 0.9 cm². (a) Overview of all three spectra. (b) Enlarged view of the Si-C, SiF₂ and Si-O-Si vibrations. (c) Enlarged view of the C-H_x vibrations.

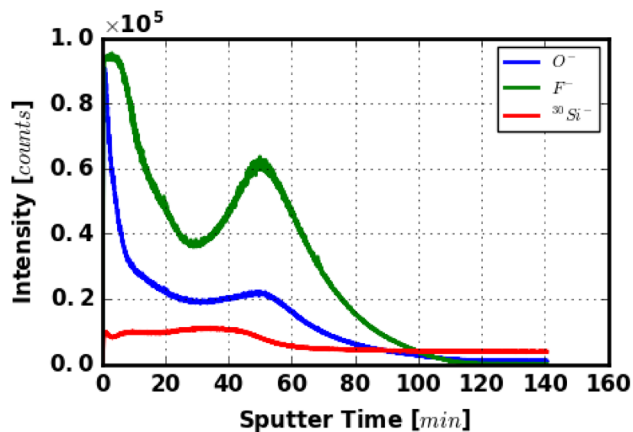


Figure 12. TOF-SIMS depth profile of a sample that was etched for 180 min (30 min periods) in 1.2 ml of 0.15 mol l⁻¹ H₂O₂ in 1.31 mol l⁻¹ HF. During etching, the C-face was exposed to the etchant, while the etched area was 0.5 cm².

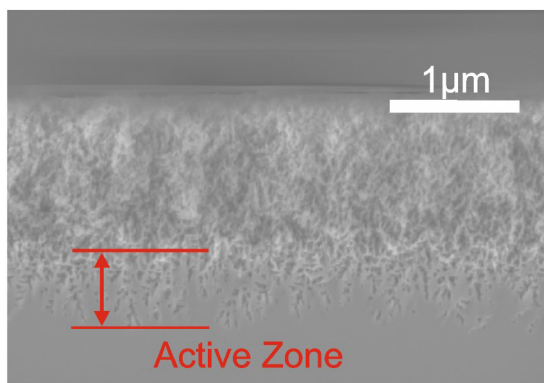


Figure 13. Cross sectional SEM micrograph corresponding to the TOF SIMS experiment illustrated in figure 12.

etching of SiC. It is also in agreement with the finding of Rittenhouse *et al*, that porous SiC obtained from MAPCE shows different photoluminescence than porous SiC obtained from pure electrochemical etching [36]. The photoluminescence is attributed to surface states, so a different surface termination is expected.

4.2. Experiments with Na₂S₂O₈

Next, the experimental results with Na₂S₂O₈ as oxidizing agent are presented. Figure 14 shows the corresponding IR-spectra while figure 15 presents the TOF-SIMS analysis and the same functional groups were identified in the IR spectra. A major difference is the relative intensity of the C–H_x peaks and the Si–O–Si peak compared to the experiments with H₂O₂. By comparison of figure 11 with figure 14 one can see that the intensity of the C–H_x peaks relative to the Si–O–Si peak is higher for the samples which were etched with H₂O₂. This indicates that the C–H_x functional groups at the surface are responsible for the passivating effect observed during MAPCE. The passivating effect is more pronounced with H₂O₂ as oxidizing agent (see figure 5—formation of line of breakage). Since the C–H_x intensity is increased as well

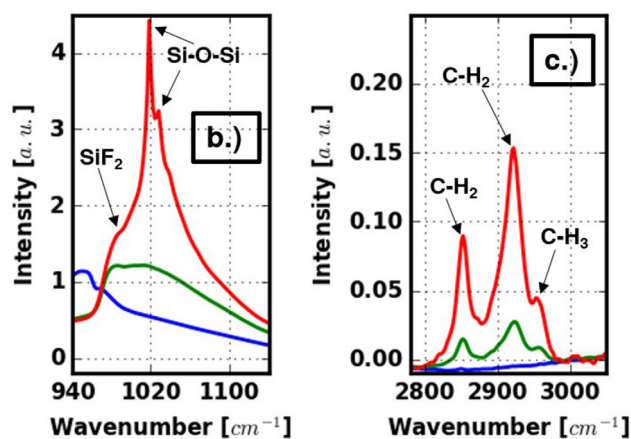
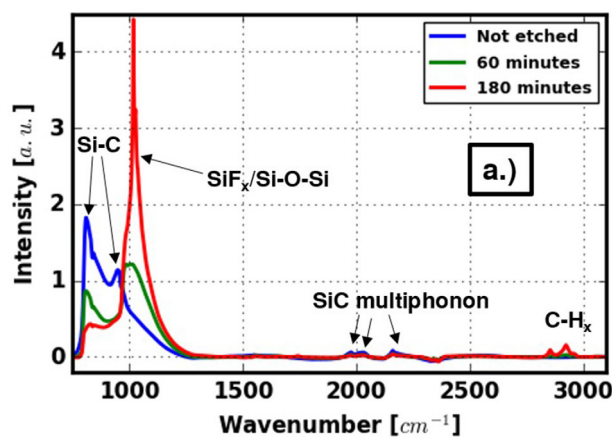


Figure 14. ATR-FTIR spectra of samples etched in 30 min MAPCE periods. Etching solution: 1.2 ml of 0.15 mol l⁻¹ Na₂S₂O₈ in 1.31 mol l⁻¹ HF. During etching, the C-face was exposed to the etchant, while the etched area was 0.9 cm². (a) Overview of all three spectra. (b) Enlarged view of the SiF₂ and Si–O–Si vibrations. (c) Enlarged view of the C–H_x vibrations.

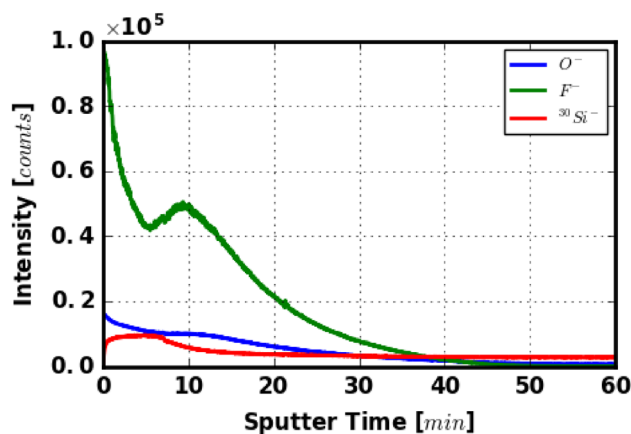


Figure 15. TOF-SIMS depth profile of a sample that was etched for 180 min (30 min periods) in 1.2 ml of 0.15 mol l⁻¹ Na₂S₂O₈ in 1.31 mol l⁻¹ HF. During etching, the C-face was exposed to the etchant, while the etched area was 0.9 cm².

when H₂O₂ is used, it is reasoned that those functional groups contribute predominantly to the observed passivating effect. This means, in turn, that they are responsible for Fermi level pinning during etching.

5. Conclusions and outlook

In this study metal assisted photochemical etching (MAPCE) of single crystalline 4H-SiC was investigated. A low power UV source (18 W) and only moderate volumes of etchant (1.2 ml) were sufficient for reliable porous layer formation. This makes this approach interesting even for large scale fabrication. Also local definition of the porous layers as well as control over the degree of porosity with depth are possible. Therefore, the goal to develop a MAPCE method that is easy to implement and which allows the preparation of uniform porous SiC layers is accomplished. Furthermore, the effect of total dissolution presents a simple and cost effective approach for micromachining 4H-SiC substrates.

Beside these findings, also fundamental knowledge about MAPCE of 4H-SiC is gained. The observed effects can be broken down to the following key statements. When exposing SiC to etching solutions containing an oxidizing agent and HF, the surface is oxidized and the oxide is dissolved by HF. The necessary holes are generated by UV light irradiation. To maintain charge neutrality during etching, electrons are transferred from the SiC via the deposited Pt electrodes into the electrolyte. There they are consumed by an oxidizing agent such as H₂O₂ or Na₂S₂O₈. Since, in turn, the UV light irradiation on the sample surface depends on the oxidizing agent concentration and etching without an oxidizing agent is not possible, these two factors strongly determine the porous layer formation during MAPCE.

A chemical analysis of the generated porous layers showed that the surface of the porous layer is covered with functional groups such as Si-O-Si, Si-F₂ or C-H_x. So oxide formation takes place during MAPCE and it is also possible that, as a side reaction, direct dissolution of SiC with F⁻ occurs as it is the case for silicon. The experiments indicate that the C-H_x groups are responsible for the passivating effect observed during MAPCE. Furthermore, there is no indication of a carbon rich layer on the surface of the MAPCE generated porous SiC, as it is often reported for electrochemical etching of SiC.

The presented findings show that the local porosification of 4H-SiC as well as controlling the degree of porosity is possible by utilizing MAPCE. Furthermore, the basic etching mechanism could be revealed. Hopefully this stimulates the realization of micro- or nanomachined device concepts based on porous silicon carbide in the near future.

Acknowledgments

This project has been supported by the COMET K1 centre ASSIC Austrian Smart Systems Integration Research Center. The COMET—Competence Centers for Excellent Technologies-Programme is supported by BMVIT, BMWFW and the federal provinces of Carinthia and Styria. The authors acknowledge the TU Wien University Library for financial support through its Open Access Funding Program’.

ORCID iDs

Stefan Schwab  <https://orcid.org/0000-0001-6531-3532>

References

- [1] Uhlir A 1956 *Bell Syst. Tech. J.* **35** 333–47
- [2] Vázsonyi É, Szilágyi E, Petrik P, Horváth Z E, Lohner T, Fried M and Jalsovszky G 2001 *Thin Solid Films* **388** 295–302
- [3] Li X and Bohn P W 2000 *Appl. Phys. Lett.* **77** 2572–4
- [4] Backes A, Bittner A, Leitgeb M and Schmid U 2016 *Scr. Mater.* **114** 27–30
- [5] Kaltsas G and Nassiopoulos A G 1997 *Microelectron. Eng.* **35** 397–400
- [6] Lyons C, Friedberger A, Welser W, Muller G, Krotz G and Kassing R 1998 *The 11th Annual Int. Workshop on Micro Electro Mechanical Systems 1998 Proc. 1998* (IEEE) pp 356–60
- [7] Armbruster S, Schafer F, Lammel G, Artmann H, Schelling C, Benzel H, Finkbeiner S, Larmer F, Ruther R and Paul O 2003 *12th Int. Conf. on IEEE Transducers, Solid-State Sensors, Actuators and Microsystems* pp 246–9
- [8] Lin V S-Y, Motesharei K, Dancil K-P S, Sailor M J and Ghadiri M R 1997 *Science* **278** 840–3
- [9] Branz H M, Yost V E, Ward S, Jones K M, To B and Stradins P 2009 *Appl. Phys. Lett.* **94** 231121
- [10] Oakes L, Westover A, Mares J W, Chatterjee S, Erwin W R, Bardhan R, Weiss S M and Pint C L 2013 *Sci. Rep.* **3** 3020
- [11] Foucaran A, Pascal-Delannoy F, Giani A, Sackda A, Combette P and Boyer A 1997 *Thin Solid Films* **297** 317–20
- [12] Du Plessis M 2008 *Mater. Sci. Eng. B* **147** 226–9
- [13] Kovalev D, Timoshenko V Y, Künzner N, Gross E and Koch F 2001 *Phys. Rev. Lett.* **87** 68301
- [14] Salonen J and Mäkilä E 2014 *Porous Silicon for Biomedical Applications* (London: Woodhead Publishing)
- [15] Rittenhouse T L, Bohn P W and Adesida I 2003 *Solid State Commun.* **126** 245–50
- [16] Leitgeb M, Backes A, Zellner C, Schneider M and Schmid U 2016 *ECS J. Solid State Sci. Technol.* **5** P148–50
- [17] Holzlechner G, Kubicek M, Hutter H and Fleig J 2013 *J. Anal. At. Spectrom.* **28** 1080–9
- [18] Konstantinov A O, Harris C I and Janzen E 1994 *Appl. Phys. Lett.* **65** 2699–701
- [19] Leitgeb M, Zellner C, Schneider M and Schmid U 2016 *ECS J. Solid State Sci. Technol.* **5** P556–64
- [20] Reiss H 1985 *J. Phys. Chem.* **89** 3783–91
- [21] Pereira V J, Weinberg H S, Linden K G and Singer P C 2007 *Environ. Sci. Technol.* **41** 1682–8
- [22] Gao Y-Q, Gao N-Y, Deng Y, Yang Y-Q and Ma Y 2012 *Chem. Eng. J.* **195** 248–53
- [23] Asoh H, Yokoyama T and Ono S 2010 *Japan. J. Appl. Phys.* **49** 46505
- [24] Tan M X, Laibinis P E, Nguyen S T, Kesselman J M, Stanton C E and Lewis N S 1994 *Prog. Inorg. Chem.* **41** 21–144
- [25] Alekseev S A, Zaitsev V N, Botsoa J and Barbier D 2007 *Chem. Mater.* **19** 2189–94
- [26] Dhar S, Seitz O, Halls M D, Choi S, Chabal Y J and Feldman L C 2009 *J. Am. Chem. Soc.* **131** 16808–13
- [27] Patrick L and Choyke W J 1961 *Phys. Rev.* **123** 813
- [28] Grill A and Neumayer D A 2003 *J. Appl. Phys.* **94** 6697–707
- [29] Peng-Fei W, Shi-Jin D, Wei Z, Jian-Yun Z, Ji-Tao W and Wei L W 2000 *Chin. Phys. Lett.* **17** 912
- [30] Langford A A, Fleet M L, Nelson A J, Asher S E, Goral J P and Mason A 1989 *J. Appl. Phys.* **65** 5154–60

- [31] Huang Z, Geyer N, Werner P, de Boor J and Gösele U 2011 *Adv. Mater.* **23** 285–308
- [32] Lauermann I, Memming R and Meissner D 1997 *J. Electrochem. Soc.* **144** 73–80
- [33] Konstantinov A O, Henry A, Harris C I and Janzen E 1995 *Appl. Phys. Lett.* **66** 2250–2
- [34] Cao T A, Luong T Q N and Dao T C 2016 *Green Process. Synth.* **5** 491–8
- [35] Petrova-Koch V, Sreseli O, Polisski G, Kovalev D, Muschik T and Koch F 1995 *Thin Solid Films* **255** 107–10
- [36] Rittenhouse T L, Bohn P W, Hossain T K, Adesida I, Lindsay J and Marcus A 2004 *J. Appl. Phys.* **95** 490–6